



# Removal of organic pollutants by zirconium containing nanoparticles: a comparative photocatalytic degradation study

Saroj Lohar<sup>1,\*</sup> , Ankita Vijay<sup>2</sup>, and Shipra Bhardwaj<sup>1,\*</sup>

<sup>1</sup> Government Meera Girls College, Mohanlal Sukhadia University, Udaipur, Rajasthan 313001, India

<sup>2</sup> Career Point University, Kota, Rajasthan, India

Received: 28 September 2020

Accepted: 30 March 2021

Published online:

22 April 2021

© The Author(s), under exclusive licence to Springer Science+Business Media, LLC, part of Springer Nature 2021

## ABSTRACT

The present work deals with the synthesis of a novel quaternary photocatalyst  $\text{ZrCdPbO}_4$ , prepared by co-precipitation method in controlled conditions. The prepared material was characterized using XRD, IR, FESEM, EDX, UV–VIS and XPS analysis to verify the crystalline nature, functional, morphological, chemical composition, band gap energy and oxidation states of elements. Generation of hydroxyl radicals was confirmed by the quenching experiment. These radicals were further used for degradation of some organic pollutants [Toluidine Blue (TB), Brilliant Green (BG) and Crystal Violet (CV)] and maximum degradation conditions like pH, concentration of dye, amount of photocatalyst and intensity of light were extracted by kinetic study. The maximum degradation rate was observed for CV =  $10.8 \times 10^{-4} \text{ (s}^{-1}\text{)}$ , for TB =  $8.62 \times 10^{-4} \text{ (s}^{-1}\text{)}$  and for BG =  $5.37 \times 10^{-4} \text{ (s}^{-1}\text{)}$ .

## Abbreviations

AOP	Advanced oxidation process
HPGA	Hierarchical porous graphene aerogels
BPA	Bisphenol A
EDX	Energy dispersive X-ray spectroscopy
FESEM	Field-emission scanning electron microscopy
IR	Infrared spectroscopy
XPS	X-ray photoelectron spectroscopy
TB	Toluidine Blue
BG	Brilliant Green
CV	Crystal Violet

## 1 Introduction

The environment is polluted by numerous human activities. It is the need of the hour to protect the environment and proceed towards sustainable development. Wang et al. [1] reviewed various processes for removal of multi-air-pollutants. One amongst the natural resources, which is getting polluted drastically, is water. Effluents from different sources like dyeing, printing, colouring industries, domestic wastewater, etc. have been continuously polluting it. Water pollution is one of the burning issues and it has drawn the attention of researchers

Address correspondence to E-mail: sarojlohar93@gmail.com; sidsidsmart@yahoo.co.in

from all over the world. Different type of pollutants like phenolic compounds, chlorophenols and other organic compounds have been degraded by different methods like biological methods [2–5], oxidation processes [6, 7], ozonation [8], radiation-induced methods, [9] etc. and these methods were used for degradation of water pollutants and several pesticides like alachlor, chlorfenvinphos, diuron, etc. Removal of carcinogenic gases like polyethylene, methanol steam reforming,  $\text{NO}_x$ , tetrachloroethylene, hydrogen sulfide, gaseous formaldehyde, gaseous acetone, toluene and *p*-xylene was carried out by advanced oxidation processes (AOP) [10–16]. Several photocatalysts are nowadays used for removal of pollutants from water sources. The effect of  $\text{TiO}_2$  on de-aromatization of *p*-toluene sulfonate was studied and the results were obtained in a time span of two hours [17].

Heterogeneous photocatalysis is an emerging technology for treatment of wastewater. The comparative study of photolytic and photocatalytic degradation of Fluvastatin (a material commonly used in cholesterol lowering drug) in presence of  $\text{ZnIn}_2\text{S}_4$  was carried out and the rate of reaction showed its removal upto 71.07% by photolysis and 99.79% by photocatalysis [18]. Other photocatalysts like  $\text{R-WO}_3/\text{TNTs}$  composite,  $\text{ZnO}$  and  $\text{TiO}_2$  [19, 20] were used for degradation and for other purposes. Co-catalysts play an important role in increasing the production of electron-hole pair at any photocatalyst's surface and their stability is also enhanced. A novel 2D material  $\text{Ti}_3\text{C}_2\text{T}_x$  ( $\text{T}_x = -\text{OH}, -\text{O}$ ) and  $\text{BiOCl}/\text{Ti}_3\text{C}_2\text{T}_x$  (named as  $\text{BT-}n$ ,  $n = 0, 0.5, 1.0, 2.0, 4.0$ ) composite materials, as co-catalysts, were synthesized by electrostatic self-assembly and used further for degradation of *p*-nitrophenol [21]. Magnetic 3D- $\text{TiO}_2$ @HPGA nanocomposites were synthesized and tested for degradation of aquatic harmful pollutants like Cr(VI) and bisphenol A (BPA) [22]. Ciprofloxacin (a chemical drug) was degraded in water, by a modified photocatalyst laponite clay-based Fe nanocomposite (Fe-Lap-RD) [23]. Ternary oxide photocatalysts give excellent results of degradation like  $\text{MoO}_3/\text{Fe}_2\text{O}_3/\text{rGO}$ ,  $\text{La}_2\text{CuO}_4/\text{CeO}_2/\text{rGO}$  and  $\text{rGO}/\text{Fe}_3\text{O}_4/\text{ZnO}$  for degradation of Methylene Blue, Reactive Blue 160 and Methylene-Violet [24–27].

Several studies reveal that quaternary photocatalytic systems are more effective than binary and ternary photocatalytic systems. Photocatalytic

activity is more improved with quaternary systems like  $\text{LaNiSbWO}_4\text{-G-PANI}$ ,  $\text{Cu}_2\text{BaSnS}_4$ , tetrahedral  $\text{CuZnInSe}_3$  nanocrystals,  $\text{GdCoSnO}_3$ ,  $\text{Cu}_2\text{ZnSnS}_4$ , etc. [28–32].

Present investigations reveal enhanced performance of prepared nanosized quaternary photocatalyst  $\text{ZrCdPbO}_4$  in removal of organic pollutants because of the following benefits over other processes:

- Use of lesser amount of photocatalyst and its reusability.
- Shorter time span required for completion of the reaction.
- Complete degradation of the pollutants.
- Use of natural renewable resource of energy that is solar energy.
- Purification of the polluted natural resource that is water.

Different characterization techniques for analysis of the photocatalyst were used and comparative studies of the degradation process were carried out.

## 2 Materials and methods

### 2.1 Synthesis of photocatalyst

A novel photocatalyst  $\text{ZrCdPbO}_4$  was prepared by co-precipitation method, from precursors (0.1 molar solutions of lead nitrate, cadmium nitrate and zirconyl nitrate each). The pH of the solution was reported 5.0 at 26 °C. The mixture was stirred continuously on a magnetic stirrer for 2 h. Pre-standardized base solution was added to the mixture with continuous stirring to obtain the precipitate. The complete precipitate was obtained at pH 10.5 and then it was allowed to settle. The obtained precipitate was filtered and washed. The supernatant liquid was checked for further precipitation. Obtained precipitate was exposed to microwave irradiation till complete liberation of various gases like  $\text{NO}_2$ ,  $\text{N}_2$ , etc. The resulting powder was then dried in the oven and was kept in the furnace for 5 h at 500 °C for calcination. Off white crystalline powder of photocatalyst  $\text{ZrCdPbO}_4$  was obtained (6.37 g). It was then characterized by EDX, XRD, IR, FESEM, UV-VIS and XPS spectroscopic analytical techniques.

## 2.2 Preparation of dye solutions

Stock solutions ( $1 \times 10^{-3}$  mol/L) of each dye [Toluidine Blue (TB), Brilliant Green (BG) and Crystal Violet (CV)] were prepared. These solutions were used as stock solutions and were diluted further to obtain the desired concentration.

## 2.3 Photocatalytic study

Stock solutions of dyes were diluted by distilled water to obtain the required concentration. 50 mL of the solution of each dye was taken in a beaker and pH of each solution was adjusted by pre-standardized NaOH and HCl. pH was recorded by pH meter (Hena pen type). The required amount of photocatalyst was added to each solution and they were exposed to a light source (200 W tungsten lamp). The changes in optical density were measured spectrophotometrically (CHINO) at different time intervals. A water filter was used to cut off thermal side reactions. Absorbance was recorded for TB, BG and CV at  $\lambda_{\text{max}} = 590$  nm, 576 nm and 625 nm, respectively.

## 2.4 Effect of pH

pH is the major factor affecting the degradation of dyes. pH of the dye solutions was varied with keeping all other factors constant and the comparative observation data are summarized in Table 1 for all the three dyes. The highest rate of degradation was obtained at pH 8.0 for TB, at 8.5 for BG and at 9.5 for CV.

## 2.5 Effect of loading dose of photocatalyst

Dose of photocatalyst is one of the factors affecting the rate of degradation. It was varied from 0.06 to 0.18 g for BG, from 0.08 to 0.20 g for TB and from 0.04 to 0.22 g for CV, while other factors were kept constant. The comparative results are summarized in Table 2.

## 2.6 Effect of concentration of dye

Concentration of all the three dyes was varied with keeping all other factors constant. The comparative data are recorded in Table 3. Depending upon absorbance, different concentrations of all the three dyes were considered to carry out the study.

**Table 1** Effect of pH on degradation rate

pH	Rate constant $\times 10^4$ ( $\text{s}^{-1}$ )		
	BG	TB	CV
5.5	2.00	0.51	1.56
6.0	2.46	3.99	3.36
6.5	2.90	4.31	3.44
7.0	3.35	5.32	3.73
7.5	3.12	7.31	4.50
8.0	4.02	<b>8.62</b>	4.50
8.5	<b>5.37</b>	6.63	8.04
9.0	4.47	6.63	8.47
9.5	3.58	5.32	<b>10.87</b>
10.0	2.76	4.08	10.44

bold values are represents highest rate constant values

## 2.7 Effect of light intensity

Light intensity is one of the factors affecting the degradation rate. The intensity of light was varied with keeping all other factors constant. Table 4 consists of the data which compares the rate of degradation for three dyes.

## 3 Results and discussion

### 3.1 Characterization

The prepared photocatalyst was characterized by different techniques. X-ray analysis was carried out in a diffraction spectrometer (Fig. 1a, model Rigaku Ultima 4, step size 0.02, scan speed  $4^\circ/\text{s}$ , voltage 40 kV and current 40 mA using Cu  $K_\alpha$  0.154 nm).

**Table 2** Effect of amount of photocatalyst on degradation rate

Amount of photocatalyst (g)	Rate constant $\times 10^4$ ( $\text{s}^{-1}$ )		
	BG	TB	CV
0.06	2.34	2.87	2.22
0.08	2.67	4.83	2.61
0.10	3.69	6.46	6.07
0.12	4.35	8.06	6.67
0.14	<b>5.37</b>	<b>8.62</b>	6.14
0.16	3.34	8.06	8.86
0.18	3.01	7.53	<b>10.87</b>
0.20	2.86	7.53	9.21
0.22	2.54	6.58	9.00

bold values are represents highest rate constant values

**Table 3** Effect of concentrations (mol/L) of dyes on degradation rate

	[BG] × 10 <sup>5</sup> M	k × 10 <sup>4</sup> (s <sup>-1</sup> )	[TB] × 10 <sup>5</sup> M	k × 10 <sup>4</sup> (s <sup>-1</sup> )	[CV] × 10 <sup>4</sup> M	k × 10 <sup>4</sup> (s <sup>-1</sup> )
	0.2	3.82	1.40	7.05	4.2	4.3
	0.4	4.61	1.50	7.84	4.4	6.4
	0.6	<b>5.37</b>	2.00	<b>8.62</b>	4.6	7.37
	0.8	4.61	2.50	7.05	4.8	<b>10.87</b>
	1.0	4.22	3.00	7.05	5.0	7.25
	1.2	3.82	3.50	5.48	5.2	6.87
	1.4	3.82	4.00	4.23	5.4	6.15
	1.6	2.32	4.20	2.82	5.6	5.6

bold values are represents highest rate constant values

**Table 4** Effect of light intensity on degradation rate

Light intensity (mW/cm <sup>2</sup> )	Rate Constant × 10 <sup>4</sup> (s <sup>-1</sup> )		
	BG	TB	CV
7.0	2.41	2.85	3.92
14.0	2.92	4.31	5.06
40.0	3.41	7.16	5.94
67.0	4.37	7.91	9.42
74.0	<b>5.37</b>	<b>8.62</b>	<b>10.87</b>

bold values are represents highest rate constant values

ZrO<sub>2</sub>, on calcinations, exists in the monoclinic phase at temperature 500 °C and at pH 10.5 [33]. The characteristic peaks of ZrO<sub>2</sub> were found at 2θ = 30.427° (111), 38.53° (200), 50.59° (220), 60.2° (311) and showed resemblance to the JCPDS (joint committee of powder diffraction standards, CAS Number 27-0997) [34]. Peaks of CdO were observed at 2θ = 34.83, 38.9°, 56.78°, 66.106° and 71.72°, having relations to (111), (200), (220), (311) and (222) planes and showed resemblance to the JCPDS (File No. 75-0594) [35, 36] and PbO at 2θ = 32.33°, 33.22°, 57.49, 69.45° and 82.18° having relations to (101), (200), (211), (220) and (310) planes [37–39]. PbO, in prepared nanomaterial, exists in orthorhombic β form as it was calcined at 500 °C [40, 41]. Average crystal size of the prepared catalyst was found to be 21.59 ± 6.15 nm which was determined using the Debye-Scherrer’s formula. The data are given in Table 5.

$$D = \frac{K\lambda}{\beta \cos \theta}$$

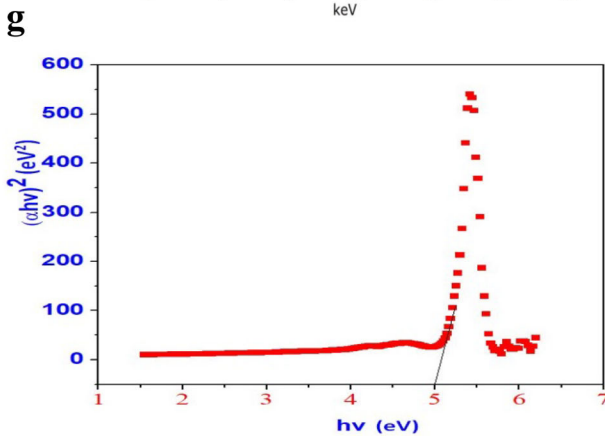
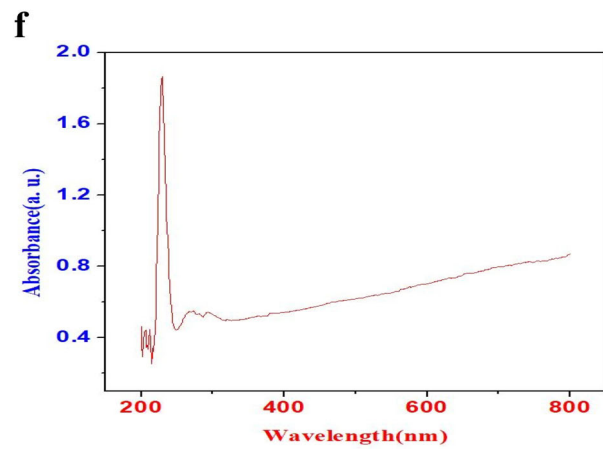
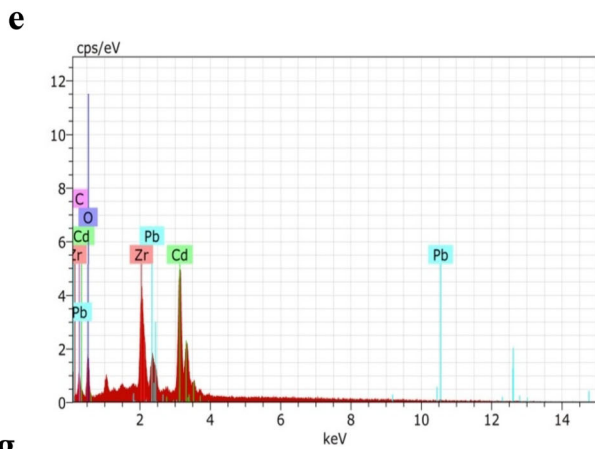
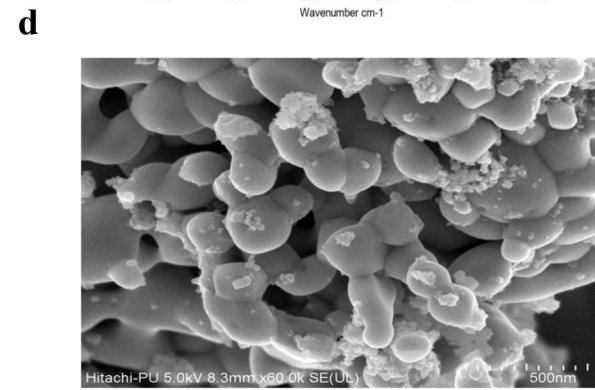
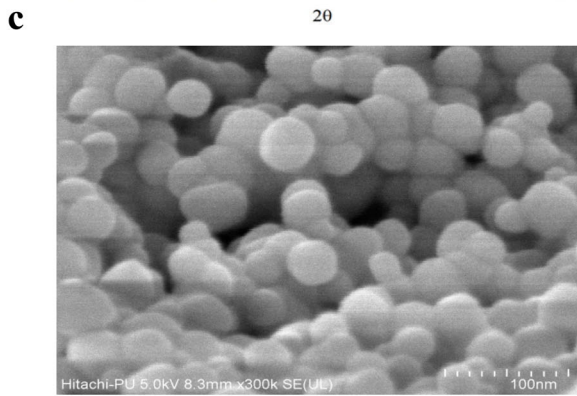
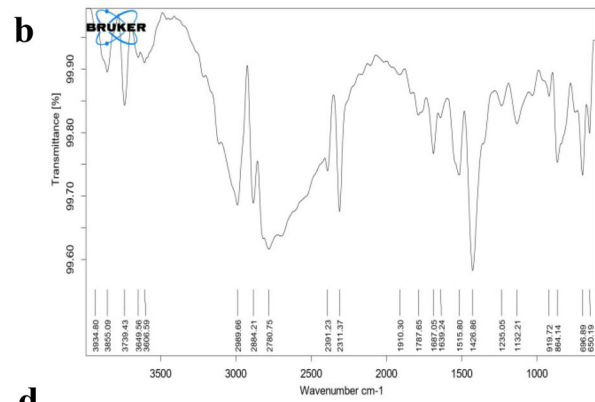
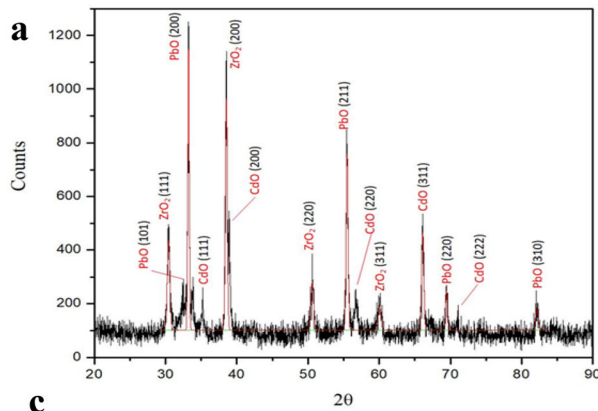
where *D* is the average crystallite size, *λ* is the X-ray wavelength (0.15406 nm). *β* is the width of the X-ray peak on the 2θ axis, full width at half maximum value (FWHM) in radians. *θ* is the Bragg angle, and *K* is the Scherrer constant (0.9).

The IR spectroscopic analysis was carried out by an infrared spectrometer (model Alpha Bruker Optik GmbH Opus) and the results obtained are given in Fig. 1b. The study suggests crystalline nano-powder nature of the prepared solid. The IR analysis shows the peaks at 3855 cm<sup>-1</sup>, 3739 cm<sup>-1</sup>, 3606 cm<sup>-1</sup> (O–H bending and stretching vibrations), 3454 cm<sup>-1</sup>, 2780 cm<sup>-1</sup>, 1426 cm<sup>-1</sup>, 919.72 cm<sup>-1</sup>, 696 cm<sup>-1</sup> and 650 cm<sup>-1</sup> (CdO stretching and bending vibrations) [42, 43], 2989 cm<sup>-1</sup>, 2391 cm<sup>-1</sup>, 2311 cm<sup>-1</sup>, 1787 cm<sup>-1</sup>, 1638 cm<sup>-1</sup>, 1515 cm<sup>-1</sup>, 1235 cm<sup>-1</sup> and 1132 cm<sup>-1</sup> (PbO stretching and bending vibrations) [44, 45] and 2884 cm<sup>-1</sup>, 1910 cm<sup>-1</sup>, 1857 cm<sup>-1</sup> and 854 cm<sup>-1</sup> (ZrO<sub>2</sub> stretching and bending vibrations) [46, 47]. A shift in peaks was observed and all peaks were sharp, indicating the presence of strong stretching vibrations and denying the presence of impurities.

The morphology of nanoparticles was examined using a field-emission scanning electron microscope (FESEM) with an accelerating voltage of 5 kV equipped with EDX (Model Hitachi PU8010). The FESEM images of ZrCdPbO<sub>4</sub> are shown in Fig. 1c, d. The presence of elements in homogeneous cluster form and arranged in an organized manner is observed. The average particle size calculated is 21.59 ± 6.15 nm.

Energy dispersive X-ray spectroscopic analysis (EDX) graph is given in Fig. 1e and reveals the presence of four elements Zr, Cd, Pb and O. The analysis suggests the presence of elements in prepared material in ratio 1.0:1.2:1.2:4.5 for Zr: Cd: Pb: O, respectively.

UV–VIS–NIR study was carried out (model lambda 750 Perkin Elmer) for the prepared compound ZrCdPbO<sub>4</sub>. The peaks obtained in the UV–VIS–NIR spectrum are at 229 nm. Figure 1f shows the



◀ **Fig. 1** Analytical techniques for characterization of ZrCdPbO<sub>4</sub>, **a** XRD spectra, **b** IR spectra, **c**, **d** FESEM images, **e** EDX spectra, **f** UV–VIS absorption spectra, **g** band gap determination plot

**Table 5** Data for calculation of crystal size

Angle (2θ)	FWHM	Crystal size	Average crystal size
30.4272	0.3798	22.1829	21.59 ± 6.15 nm
32.7234	0.3024	25.2068	
33.2249	0.2091	36.3947	
34.9785	0.3213	23.5824	
38.5378	0.2830	26.4925	
50.5968	0.4132	17.3823	
55.4969	0.2813	24.9909	
57.2584	0.4314	16.1786	
60.0698	0.4519	15.2167	
66.1063	0.3053	21.8100	
69.4566	0.2861	22.8178	
71.2285	0.5054	12.7787	
82.1838	0.3370	17.7616	

absorption spectra. Band gap of ZrCdPbO<sub>4</sub> was determined by Tauc relation [48]:

$$\alpha hv = A(hv - E_g)^n,$$

where  $\alpha$  is absorption coefficient,  $E_g$  is optical band gap,  $A$  is constant,  $h\nu$  is photon energy and  $n = 1/2$  for direct transitions.

A graph (Fig. 1g) is plotted between  $h\nu$  and  $(\alpha hv)^2$ . The extrapolation of straight line to  $(\alpha hv)^2 = 0$  gives the value of optical band gap of prepared photocatalyst. Band gap energy is calculated using the wave energy formula [49]:

$$E_g = \frac{hc}{\lambda} (eV),$$

where  $h$  is the Planck's constant,  $c$  is the velocity of light and  $\lambda$  is the wavelength of the sample.

Band gap energy of the prepared photocatalyst was found to be 5.0 eV [50, 51]. Calculation from methods, Tauc relation and wave energy formula, gave the same values of the band gap.

XPS analysis is employed for the estimation of electronic and chemical states of prepared material. The analysis is carried out on an instrument model SOFH PHI versa probe III. A monochromatic X-ray source Al K<sub>α</sub> (1486.6 eV) is used with FAT mode with power of 24.65 W and sputter ion Ar<sup>+</sup>. The source

analyzer angle is 45.0°, deconvolution pass energy is 6.50 eV with energy step 20 meV. The whole data were analyzed on software version SS2.7.1.22. The result shown in Fig. 2 represents the full XPS spectrum of prepared material and confirms the presence of relevant elements. The peaks observed for Cd4d, Pb4f, Zr3d, C1s, Zr3p, Cd3d, Pb4d, O1s, Cd3p, Pb4p reveal the presence of Zr, Cd, Pb and O. Observation data are summarized in Table 6 showing relative core level splitting and their binding energy.

The peaks were observed for the core level spectrum (Fig. 3a) of Zr3d components of spin-orbit splitting (3d<sub>5/2</sub> and 3d<sub>3/2</sub>) with binding energy at 179.3 eV and 181.55 eV. Difference of energy between two peaks is 2.25 eV which favors the presence of Zr<sup>4+</sup> [52]. It is observed that Zr3d peaks are shifted to the lower binding energy side as compared to the pure Zr3d peaks with the binding energy range of 182.1 to 182.8 eV [53]. A core level spectrum of Cd 3d is shown in Fig. 3b with spin-orbit components 3d<sub>5/2</sub> and 3d<sub>3/2</sub> at 402.15 eV and 408.9 eV. These binding energies are observed in lower range from the standard value of pure CdO nanocrystal which exists at 405.0 and 411.7 eV [54]. This shifting occurs due to the chemical environment of other metal ions. Energy difference between two splitting is 6.75 eV which confirms the presence of Cd<sup>2+</sup> [55, 56]. Pb 4f doublet peaks are correlated to spin-orbit splitting of 4f<sub>7/2</sub> and 4f<sub>5/2</sub> which are observed at 135.05 and 140.1 eV and core level spectrum is shown in Fig. 3c. The value of 4f<sub>7/2</sub> is much closer to the standard value which represents bonding of Pb<sup>2+</sup> [57, 58]. The energy separation between 4f doublet peaks is found 5.05 eV which is due to Pb–O, suggesting that Pb<sup>2+</sup> was bonded with the oxygen group [59, 60].

Figure 3d and e represent O1s spectrum and deconvolution form of O1s into three peaks. It is evident that the peak at 529.7 eV is related to the oxygen anions O<sup>2-</sup> bonded to metal cations [61]. Three metal cations, in the prepared material, are bonded with oxygen. Thus, in 1s spectrum of oxygen, three peaks are observed at 528.2, 528.4 and 528.7 eV, which are of equal intensity and which have less energy difference. These peaks correspond to Zr–O<sub>2</sub>, Cd–O and Pb–O bonds. The binding energy for Pb(II) is found in the range 527.8–529.5 eV in complexes having activated carbon [62]. Lower binding energy correlates to the presence of O<sup>2-</sup> and justifies the presence of Cd–O bond [63]. The binding energy peak of 1 s for oxygen and 1 s for carbon in Zirconia

**Fig. 2** XPS spectrum of prepared material

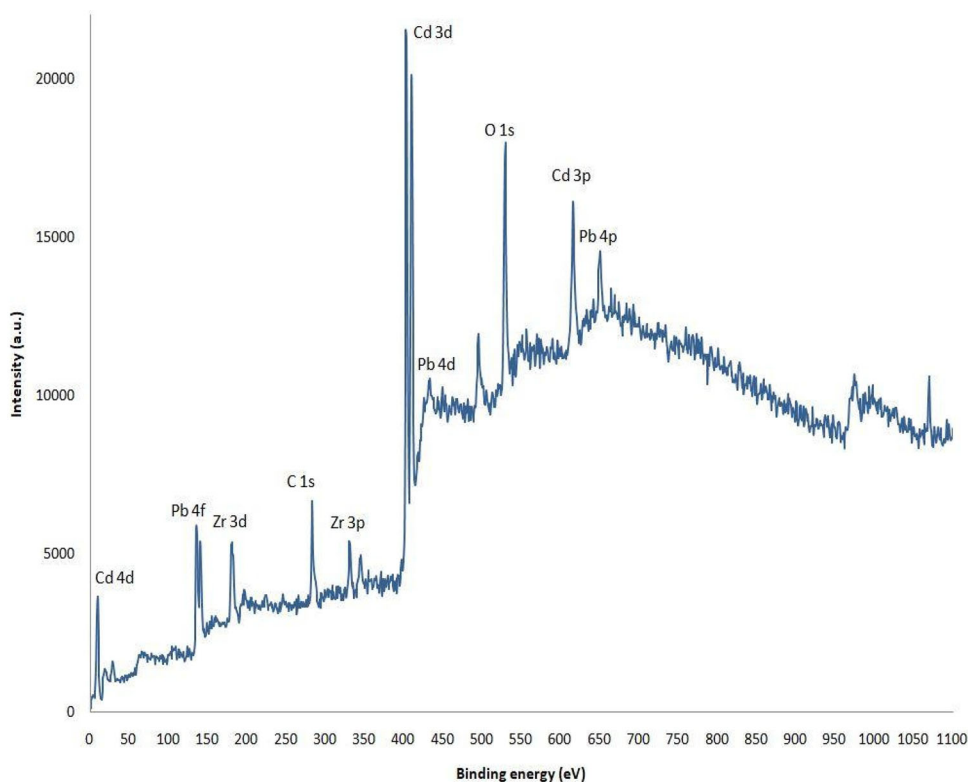


**Table 6** Observation data of XPS spectrum for prepared material

Elements	Spin-orbit components	Observed binding energy (eV)	Energy difference (eV)
Zr	3d <sub>5/2</sub>	179.3	2.25
	3d <sub>3/2</sub>	181.55	
Cd	3d <sub>5/2</sub>	402.15	6.75
	3d <sub>3/2</sub>	408.9	
Pb	4f <sub>7/2</sub>	135.05	5.05
	4f <sub>5/2</sub>	140.1	
O	1s	528.2–528.7	–

is located at 528.23 eV and 284.64 eV, respectively [64].

### 3.2 A typical run

A plot between time and  $1 + \log OD$  for all the three dyes was drawn and is given in Fig. 4. It was found to be a straight line suggesting that the reaction follows pseudo first order kinetics in case of all the three dyes. A comparative study shows that CV is degraded faster than other BG and TB. Effects of various operational parameters on degradation rate were studied. Rate constant for degradation was calculated as follows:

$$k = 2.303 \times \text{slope.}$$

The maximum degradation rate obtained, at certain values of parameters (Table 7), is for CV =  $10.8 \times 10^{-4} \text{ (s}^{-1}\text{)}$ , for TB =  $8.62 \times 10^{-4} \text{ (s}^{-1}\text{)}$  and for BG =  $5.37 \times 10^{-4} \text{ (s}^{-1}\text{)}$ .

Percentage of dye degradation was evaluated for all three dyes on optimum conditions of parameters by equation:

$$\text{Degradation efficiency (DE) (\%)} = \frac{A_0 - A_t}{A_0} \times 100,$$

where  $A_0$  and  $A_t$  are the absorbance at initial time and at time  $t$ , respectively.

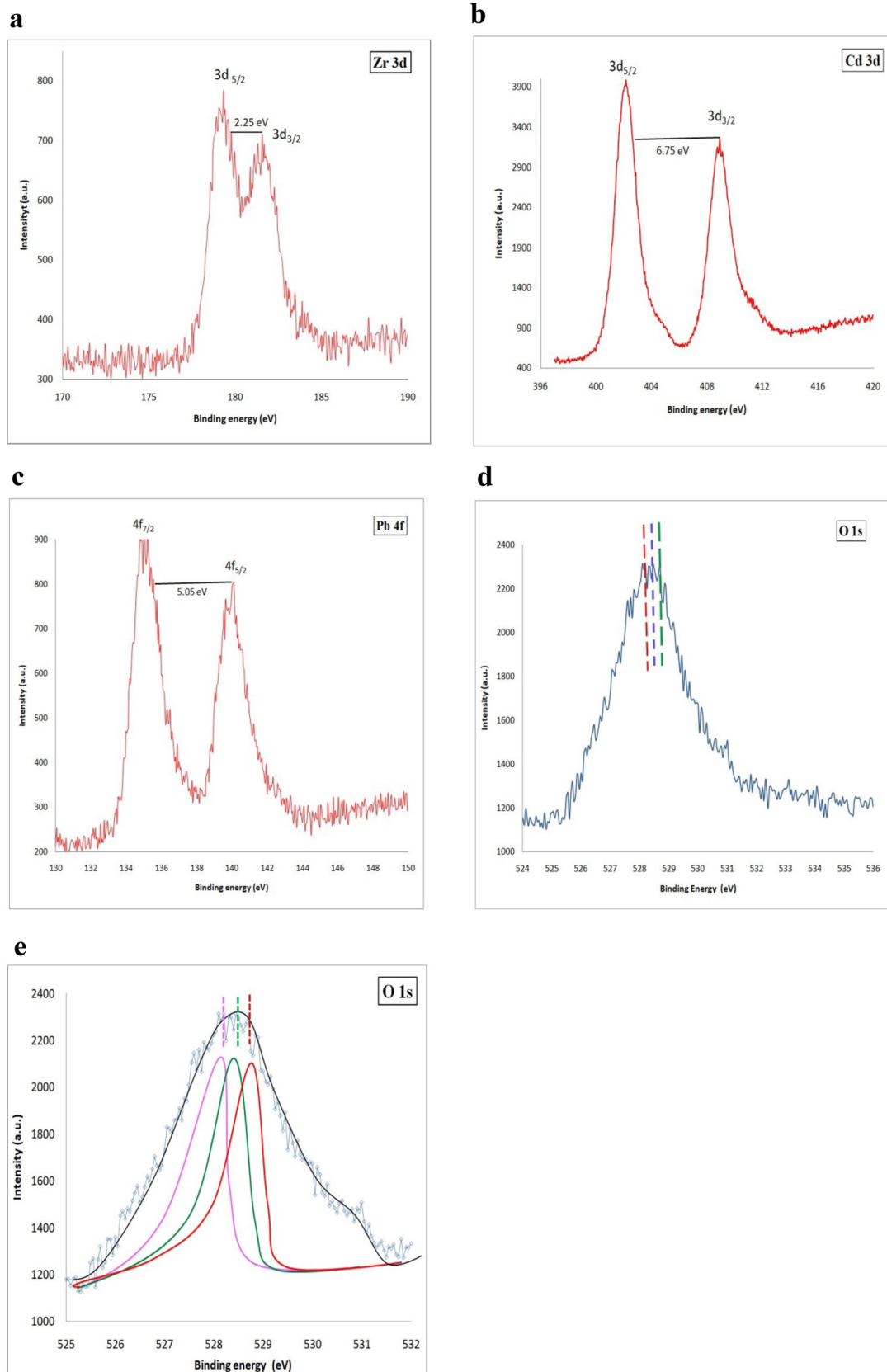


**Fig. 3** XPS spectra of **a** Zr 3d, **b** Cd 3d, **c** Pb 4f, **d** O 1s and **e** deconvoluted of O 1s



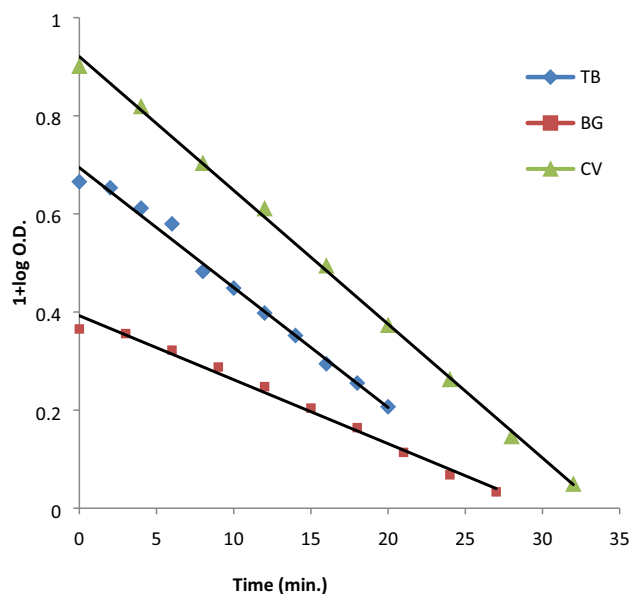


**Fig. 4** Typical runs for all three dyes

Photocatalytic degradation efficiency calculated for CV is 88.88% in 32 min, for TB is 78.91% in 30 min and for BG is 74.78% in 40 min.

### 3.3 Effect of pH

pH is the major factor affecting the degradation of dyes. It was observed that with change in pH, the initial optical density of the solution changes, which can also be observed in multi line graphs, suggesting the pH sensitive nature of dyes. Comparative results are reported in Fig. 5a–c for all the three dyes. Rate of degradation increases with increase in pH of the solution. It may be explained on the basis that as pH rises, concentration of  $\text{OH}^-$  ions increases. Electrons from these ions are abstracted by the holes, which are generated at the surface of photocatalyst by absorbance of photons, converting these ions into hydroxyl radicals  $\cdot\text{OH}$ . These hydroxyl radicals are responsible

for degradation of the dye molecules which is also confirmed by scavenger study. After attaining maxima, rate of reaction decreases with increase in concentration of  $\text{OH}^-$  ions as the generated  $\text{OH}^-$ -free radicals, with increase in their concentration, now experience repulsion amongst themselves and with cationic surface of dyes. Thus, the rate of degradation decreases.

### 3.4 Effect of loading dose of photocatalyst

Dose of photocatalyst is one of the factors affecting the rate of degradation. The effects of dose of photocatalyst are graphically represented in Fig. 6a–c. The effect can be attributed to the fact that with increase in amount of photocatalyst, surface area of photocatalyst increases, thus a greater number of hole-electron pairs are generated at its surface by absorbing photons of light. This produces more  $\cdot\text{OH}$ -free radicals and rate of degradation is enhanced. Further increase in the amount of photocatalyst generates a greater number of hole-electron pairs, making the place crowded and forcing recombination of them. Thus, reduction in degradation rate is observed.

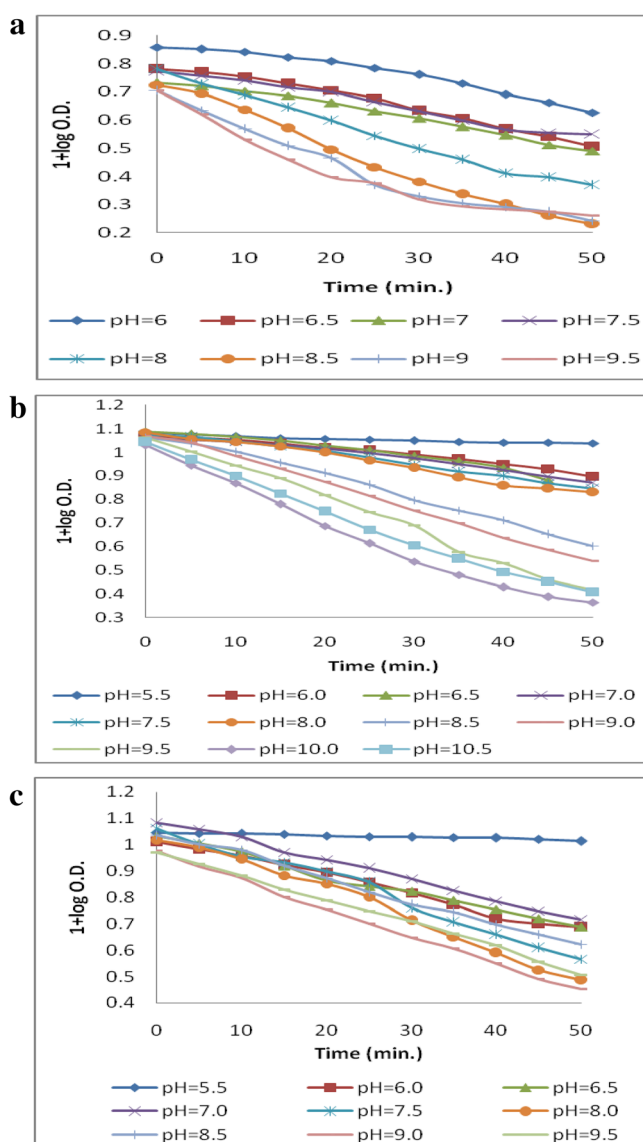
### 3.5 Effect of concentration of dye

Concentration of pollutants is a factor to be considered for treatment of wastewater. Figure 7a–c shows the effect of various concentrations on degradation rate. It was observed that the rate of degradation increases with increase in concentration of dye. It is since more dye molecules are available to absorb photons from light and get excited. These molecules, on reaction with  $\text{OH}^-$ -free radicals, break down into fragments and thus, rate of degradation increases. Further with increase in concentration of dye molecules, they themselves start acting as a filter to the

**Table 7** Maximum degradation conditions for all three dyes

Factors↓	BG	TB	CV
Rate of degradation ( $\text{s}^{-1}$ )→	$5.37 \times 10^4$	$8.62 \times 10^4$	$10.8 \times 10^4$
pH	8.5	8.0	9.5
Dose of photocatalyst (g)	0.14	0.14	0.18
Concentration of dye (mol/L)	$0.6 \times 10^5$	$2.0 \times 10^5$	$4.8 \times 10^4$
Light intensity ( $\text{mW}/\text{cm}^2$ )	74.0	74.0	74.0
Degradation efficiency (%)	74.78	78.91	88.88

**Fig. 5** Effect of variation of pH for **a** BG, **b** TB and **c** CV



incident light and do not permit desired wavelength to reach the surface of photocatalyst particles. Thus, decrease in rate of degradation is observed.

### 3.6 Effect of light intensity

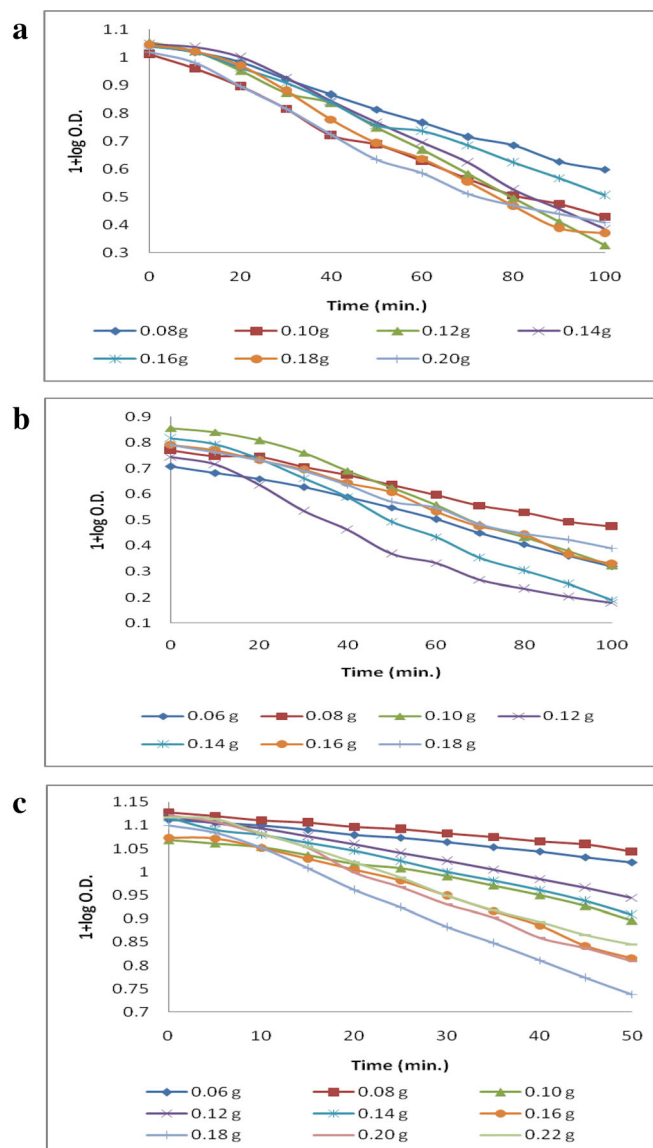
Light intensity is one of the factors affecting the degradation rate. Figure 8a–c consists of the data of effect of light intensity. It was observed in all the three cases that with increase in light intensity, rate of degradation increases because more photons are available to strike onto the photocatalyst crystals surface and dye molecules. Thus, a greater number of dye molecules get excited and get degraded. Further

higher light intensities were not considered due to occurrence of some thermal side reactions.

### 3.7 Scavenger study

Scavenger study, in presence of light and photocatalyst for all three dyes, was carried for interpretation of the degradation mechanism. Different scavengers were used to rule out the species taking part in degradation. The data are graphically reported in Fig. 9. It is evident from the data that addition of isopropyl alcohol (hydroxyl radical scavenger) ceases the reaction efficiently (up to 90%), as compared to other scavengers, confirming the role of OH-free radicals as active oxidizing species in the reaction.

**Fig. 6** Effect of dose of photocatalyst for **a** BG, **b** TB and **c** CV



### 3.8 A comparative analysis

Effect of various factors on degradation of all the three dyes was studied and it was observed that degradation rate is higher for CV in comparison to BG and TB. This is explained on the basis of chemical structures, bond strength and effect of ring strain in dye molecules. Figure 10 contains the chemical structure of TB, BG and CV. TB is more stable because its azo groups are stabilized by resonance. Therefore, breaking bonds in TB requires more energy and degradation of TB takes longer time. On the other hand, the structure of CV has ring strain, which is distributed in aryl groups, thus breaking bonds in it becomes easier. BG is a bulky molecule as

compared to the other two and degradation of it requires greater time. Thus, the order of degradation is ruled out as: CV > TB > BG with rate constant  $10.8 \times 10^{-4} > 8.62 \times 10^{-4} > 5.37 \times 10^{-4}$  ( $s^{-1}$ ), respectively.

### 3.9 Mechanism

A tentative mechanism is proposed for all the three dyes.

(1)

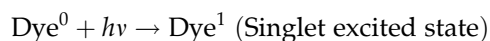
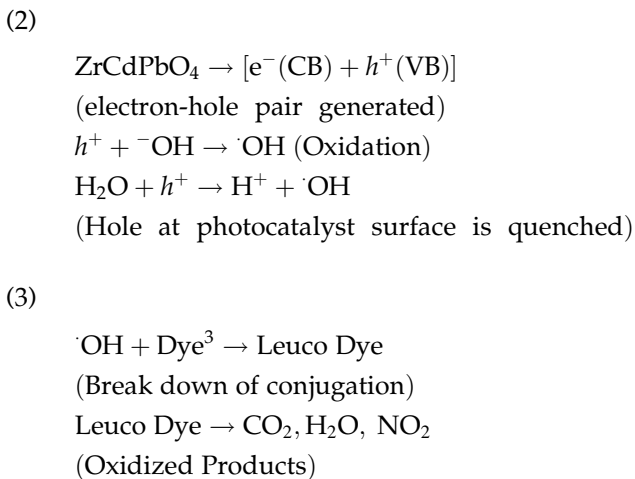
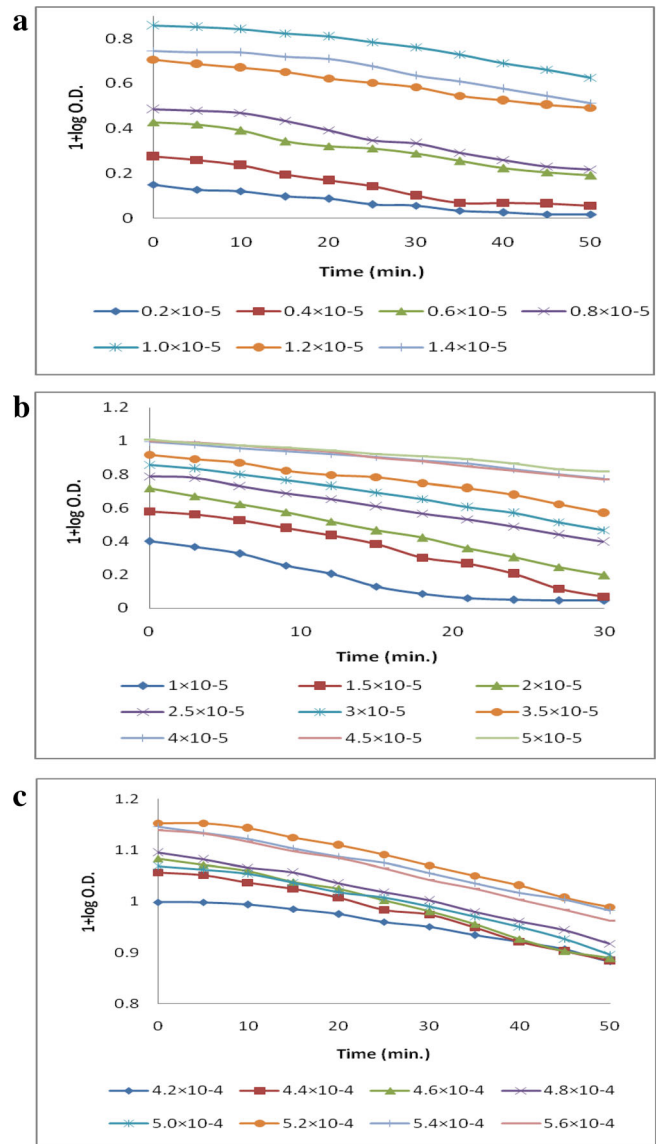


**Fig. 7** Effect of concentrations (mol/L) of **a** BG, **b** TB and **c** CV



where  $h\nu$  is light photon and ISC is inter system crossing.

Mechanism shows that electron-hole pairs, generated at the photocatalyst surface, participate in redox reactions. The scavenger study suggests formation of  $\cdot\text{OH}$ -free radical which is generated by abstraction of an electron from  $\text{OH}^-$  ions. Hydroxyl-free radicals oxidize the organic dye. A chain reaction starts by breakdown of conjugation resulting in complete mineralization of dye molecules. The by-products of the reaction are  $\text{NO}_2$ ,  $\text{CO}_2$ ,  $\text{H}_2\text{O}$ , etc.

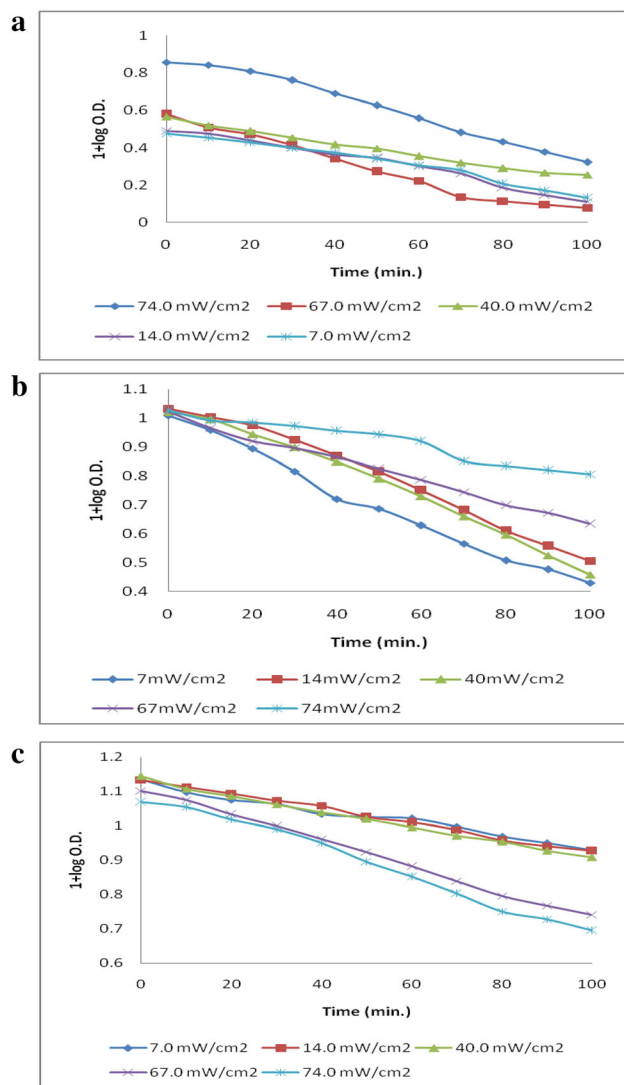


**Fig. 8** Effect of light intensity for **a** BG, **b** TB and **c** CV

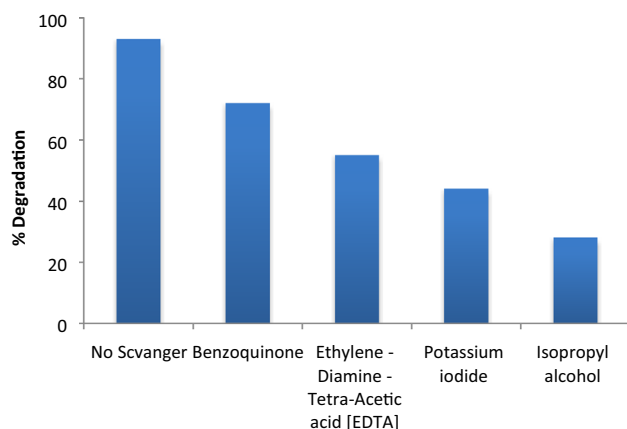


**Fig. 9** Effect of various scavengers on the degradation of dyes (concentration of BQ, EDTA, KI, IPA = 1 mol/L)

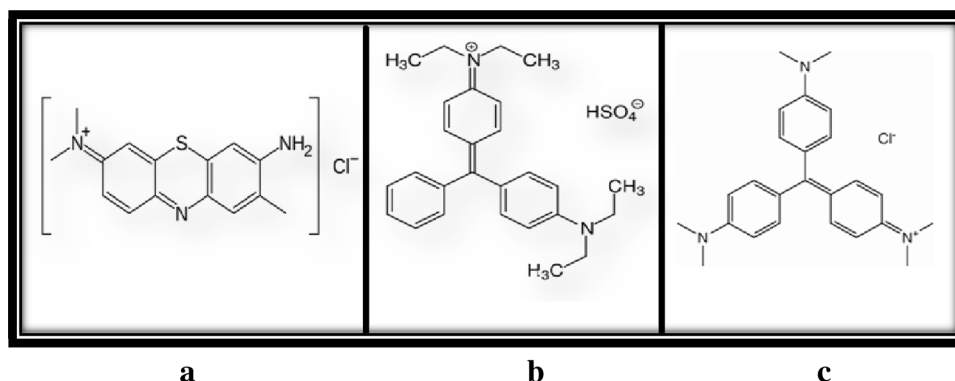
## 4 Conclusions

The quaternary photocatalyst  $\text{ZrCdPbO}_4$  was synthesized and was characterized by different analytical techniques that are XRD, IR, FESEM, EDX, UV-VIS and XPS analysis. This photocatalyst was further used for mineralization of dyes Crystal Violet, Brilliant Green and Toluidine Blue. A comparative study was also carried out which showed that the photocatalyst works more effectively over CV than the other two. The photocatalytic mineralization is found to be a superior process over others in the following manner:

- Use of solar light makes the process inexpensive as far as energy usage is concerned.
- Photocatalyst is prepared by a simple precipitation method and does not add any pollutant to the environment.
- Reusability of the photocatalyst makes the process economic one.
- The technique removes pollutants from water completely, purifying it. Although treated water cannot be used for drinking purpose but may be used for irrigation, washing, cleaning, cooling and other purposes.
- The process does not add any pollutant or degraded product to the environment thus protecting it from further pollution.
- Minute amount of photocatalyst can purify the water at large scale.
- Separation of photocatalyst from the source can be done by simple filtration as the phase is heterogeneous.
- Regeneration of photocatalyst can be done by a simple chemical process and calcination.

Thus, in current scenario, the process sounds to be easier, superior and most beneficial one to the society over other processes.

**Fig. 10** Chemical structure of dyes **a** Toluidine Blue, **b** Brilliant Green, **c** Crystal Violet



## Acknowledgements

Authors are thankful to Professor S.C. Ameta, Director, Department of Applied Sciences, PAHER University, Udaipur, India for his valuable guidance and support. Authors are also thankful to SAIF and CIL laboratory, Punjab University, Chandigarh, India and College of Science, MLSU, Udaipur, India for carrying out the analysis.

## Funding

The authors did not receive support from any organization for the submitted work.

## Declarations

**Conflict of interest** The authors declare that they have no conflict of interest.

## References

- H. Wang, B. Yuan, R. Hao, Y. Zhao, X. Wang, *Chem. Eng. J.* **378**, 122–155 (2019)
- A.M. Amat, A. Arques, H. Beneyto, A. Garcia, M.A. Miranda, S. Segui, *Chemosphere* **53**(1), 79–86 (2003)
- E. Tamer, Z. Hamid, A.M. Aly, E.T. Ossama, M. Bo, G. Benoit, *Chemosphere* **63**(2), 277–284 (2006)
- M.C. Diez, *J. Soil Sci. Plant Nutr.* **10**(3), 244–267 (2010)
- S.S. Phugare, D.C. Kalyani, Y.B. Gaikwad, J.P. Jadhav, *Chem. Eng. J.* **230**, 27–35 (2013)
- R. Hao, X. Mao, Z. Wang, Y. Zhao, T. Wang, Z. Sun, B. Yuan, Y. Li, *J. Hazard. Mater.* **368**, 224–234 (2019)
- A. Mojiri, A. Ohashi, N. Ozaki, A. Shoiful, T. Kindaichi, *Int. J. Environ. Res. Public Health* **15**, 1443 (2018)
- M.I. Maldonado, L.A. Perez-Estrada, W. Gernjak, I. Oller, X. Domenech, J. Peral, J. Hazard. Mater. **138**(2), 363–369 (2006)
- N. Getoff, *Radiat. Phys. Chem.* **47**, 581–593 (1996)
- J. Konar, R. Ghosh, S. Ghosh, *Polym. Degrad. Stab.* **22**(1), 43–52 (1988)
- J. He, Z. Yang, L. Zhang, Y. Li, L. Pan, *Int. J. Hydrogen Energ.* **42**(15), 9930–9937 (2017)
- T. Maggos, J.G. Bartzis, M. Liakou, C. Gobin, *J. Hazard. Mater.* **146**(3), 668–673 (2007)
- G.E. Imoberdorf, H.A. Irazoqui, A.E. Cassano, O.M. Alfano, *Ind. Eng. Chem. Res.* **44**(16), 6075–6085 (2005)
- S. Limtrakul, S. Rojanamatin, T. Vatanatham, P.A. Ramachandran, *Ind. Eng. Chem. Res.* **44**(16), 6115–6122 (2005)
- T. Noguchi, A. Fujishima, P. Sawunyama, K. Hoshimoto, *Environ. Sci. Technol.* **32**(23), 3831–3833 (1998)
- W.J. Liang, J. Li, Y.Q. Jin, *J. Environ. Sci. Health A Toxic Hazard. Subst. Environ. Eng.* **45**(11), 1384–1390 (2010)
- P. Cesar, K. John, *C.H.I.M.I.A. Int. J. Chem.* **50**(3), 50–55 (1996)
- T. Liu, L. Wang, C. Sun, X. Liu, R. Miao, Y. Lv, *Chem. Eng. J.* **358**, 1296–1304 (2019)
- X. Wang, M. Sun, M. Murugananthan, Y. Zhang, L. Zhang, *Appl. Catal. B: Environ.* **260**, 118205 (2020)
- S. Sakthivel, B. Neppolian, M.V. Shankar, B. Arabindoo, M. Palanichamy, V. Murugan, *Sol. Energy Mater. Sol. Cells* **77**(1), 65–82 (2003)
- C. Wang, J. Shen, R. Chen, F. Cao, B. Jin, *Appl. Surf. Sci.* **519**, 146175 (2020)
- C. Santhosh, A. Malathi, E. Daneshvar, P. Kollu, A. Bhatnagar, *Sci. Rep.* **8**, 15531 (2018)
- M. Bobu, A. Yediler, I. Siminiceanu, S. Schulte-Hostede, *Appl. Catal. B: Environ.* **83**, 15–23 (2008)
- R.B. Anjaneyulu, B.S. Mohan, G.P. Naidu, R. Muralikrishna, *J. Asian Ceram. Soc.* **6**, 183–195 (2018)

25. S. Shanavas, A. Priyadharsan, V. Vasanthakumar, A. Arunkumar, P.M. Anbarasan, S. Bharathkumar, J. Photochem. Photobiol. A Chem. **340**, 96–108 (2017)
26. S. Thangavel, S. Thangavel, N. Raghavan, K. Krishnamoorthy, G. Venugopal, J. Alloys Compd. **665**, 107–112 (2016)
27. Q.A. Drmosh, A. Hezam, A.H. Hendi, M. Qamar, Z.H. Yamani, K. Byrappa, Appl. Surf. Sci. **499**, 143938 (2020)
28. M.R. Biswas, K.Y. Cho, C.H. Jung, W.H. Oh, Process Safety Environ. Protection **126**, 348–355 (2019)
29. A. Ali, S. Ahmed, J. Rehman, M.R. Abdullhah, H.B. Chen, B. Guo, Y. Yang, Mater. Today Commun. 101675 (2020)
30. D. Li, J. Yang, W. Qi, Q. Gao, J. Alloys Compd. **854**, 157096 (2021)
31. I. Muneer, M.A. Farrukh, D. Ali, F. Basher, Mater. Sci. Eng.: B **265**, 115028 (2021)
32. Z. Hou, Y. Li, J. Liu, H. Shen, X. Huo, New J. Chem **45**, 1743–1752 (2021)
33. Yu.V. Kolen'koa, V.D. Maximova, A.A. Burukhinb, V.A. Muhanovb, B.R. Churagulovb, Mater. Sci. Eng. C **23**, 1033–1038 (2003)
34. N. Pal, A. Bhaumik, Dalton Trans. **41**, 9161–9169 (2012)
35. A.N. Abd, M.O. Dawood, M.H. Hassoni, A.A. Hussein, World Sci. News **37**, 249–264 (2016)
36. W.M. Abdulridha, Int. J. Nano Chem. **2**, 1–9 (2016)
37. M. Suganya, A.R. Balu, K. Usharani, Mater. Sci. Poland **32**(3), 448–456 (2014)
38. M.K. Mahmoudabad, M.M. Kashani-Motlagh, Int. J. Phys. Sci. **6**(24), 5720–5725 (2011)
39. H. Karami, M.A. Karimi, S. Haghdar, Mater. Res. Bull. **43**, 3054–3065 (2008)
40. S.A. Elawam, W.M. Morsi, H.M. Abou-Shady, O.W. Guirguis, Brit. J. Appl. Sci. Technol. **17**(1), 1–10 (2016)
41. R. Yousefi, F.J. Sheini, A. Sa'aedi, M. Cheraghizade, Sains Malaysiana **44**(2), 291–294 (2015)
42. A.S. Aldwayyan, F.M. Al-Jekhedab, M. Al-Noaimi, B. Hammouti, T.B. Hadda, M. Suleiman, I. Warad, Int. J. Electrochem. Sci. **8**, 10506–10514 (2013)
43. K. Kaviyarasu, E. Manikandan, P. Paulraj, S.B. Mohamed, J. Kennedy, J. Alloys Compd. **593**, 67–70 (2014)
44. M. Alagar, T. Theivasanthi, A.K. Raja, J. Appl. Sci. **12**, 398–401 (2012)
45. M.A. Rezvani, S. Khandan, N. Sabahi, Energy Fuels **31**, 5472–5481 (2017)
46. G.K. Sidhu, A.K. Kaushik, S. Rana, S. Bhansali, R. Kumar, Appl. Surf. Sci. **334**, 216–221 (2014)
47. S.M. Yakout, H.S. Hassan, Molecules **19**, 9160–9172 (2014)
48. K. Manickathai, S.K. Viswanathan, M. Alagar, Indian J. Pure Appl. Phys. **46**, 561–564 (2008)
49. K.T. Arulmozhi, N. Mythili, AIP Adv. **3**, 122122 (2013)
50. I. Kosacki, V. Petrovsky, H.U. Anderson, Appl. Phys. Lett. **74**(3), 341 (1999)
51. B. Kralik, E.K. Chang, S.G. Louie, Phys. Rev. B **57**(12), 7027–7036 (1998)
52. M.R. Shaik, M. Alam, S.F. Adilo, M. Kuniyil, A. Al-Warthan, M.R. Siddiqui, M.N. Tahir, J.P. Labis, M. Khan, Materials **12**, 711 (2019)
53. C.V. Reddy, B. Babu, I.N. Reddy, J. Shim, Ceram. Int. **44**, 6940–6948 (2018)
54. F.T. Thema, P. Beukes, A. Gurib-Fakim, M. Maaza, J. Alloys Compd. **646**, 1043–1048 (2015)
55. S. Majumder, A.C. Mendhe, D. Kim, B.R. Sankapal, J. Alloys Compd. **788**, 75–82 (2019)
56. P. Sakthivel, S. Asaithambi, M. Karuppaiah, S. Sheikfareed, R. Yuvakkumar, G. Ravi, J. Mater. Sci. Mater. Electron. **30**, 9999–10012 (2019)
57. P.X. Sheng, Y. Ting, J.P. Chen, L. Hong, J. Colloid Interface Sci. **275**, 131–141 (2004)
58. A. Swiatkowski, M. Pakula, S. Biniak, M. Walczyk, Carbon **42**, 3057–3069 (2004)
59. L.J. Chen, S.M. Zhang, Z.S. Wu, Z.J. Zhang, H.X. Dang, Mater. Lett. **59**, 3119–3121 (2005)
60. S. Zhang, H. Yang, H. Huang, H. Gao, X. Wang, R. Cao, J. Li, X. Xu, X. Wang, J. Mater. Chem. A **5**, 15913–15922 (2017)
61. W. Zou, R. Han, Z. Chen, J. Shi, L. Hongmin, J. Chem. Eng. Data **51**, 534–541 (2006)
62. A.M. Soliman, S.A. Elsuccary, I.M. Ali, A.I. Ayeshe, J. Water Process. Eng. **17**, 245–255 (2017)
63. A.V. Moholkar, G.L. Agawane, K. Sim, Y. Kwona, D.S. Choi, K.Y. Rajpure, J.H. Kim, J. Alloys Compd. **506**, 794–799 (2010)
64. M. Ramachandran, R. Subadevi, W. Liu, M. Sivakumar, J. Nanosci. Nanotechnol. **18**, 368–373 (2018)

**Publisher's note** Springer Nature remains neutral with regard to jurisdictional claims in published maps and institutional affiliations.